Supplementary Material to Manuscript Scaling and exceedance probability of sinkhole collapse in evaporite karst (Dead Sea, Jordan)

Hanna Z. Schulten^{1*}, Robert A. Watson^{1*}, Djamil Al-Halbouni² & Eoghan P. Holohan^{1,3}

¹ UCD School of Earth Sciences, University College Dublin, Dublin, Ireland

²Institute of Earth System Sciences and Remote Sensing, Leipzig University, Leipzig, Germany

³iCRAG - Research Ireland Centre for Applied Geosciences, University College Dublin, Dublin, Ireland

Supplementary Tables

Table S1: Satellite and aerial image metadata. Showcases the temporal information of the images as well as the off-nadir view angle and collection azimuth. (RJGC = Royal Jordanian Geographical Centre). The ground sample distance refers to the side length of one image pixel as it relates to the land/lake surface.

Year	Sensor/Source	Date Acquired	Acquisition Time (UTC)	Off-Nadir View Angle (°)	Collection Azimuth	Ground sample distance (m)
1967	Corona (USGS)	n/a	n/a	n/a	n/a	n/a
1992	Airborne Camera (RJGC)	n/a	n/a	n/a	n/a	n/a
2000	Airborne Camera (RJGC)	n/a	n/a	n/a	n/a	n/a
2002	Quickbird	2002-06-19	08:14	25.4	62.6	0.61
2002	Quickbird	2002-07-07	08:14	25.1	106.3	0.61
2004	Quickbird	2004-10-20	08:21	12	90.1	0.61
2005	Quickbird	2005-10-28	08:37	3.3	120.1	0.61
2006	Quickbird	2006-11-18	08:42	11	131.3	0.61
2007	Quickbird	2007-08-28	08:43	13.8	161.9	0.61
2008	Worldview 1	2008-04-20	08:26	18.3	240.3	0.5
2009	GeoEye-1	2009-08-09	08:32	19.3	223.9	0.5
2010	GeoEye-1	2010-07-29	08:27	13.2	226.3	0.5
2011	Worldview 1	2011-08-26	08:38	5.2	104.7	0.5
2012	Quickbird	2012-03-05	07:42	19.8	119	0.61
2013	Pleiades-1A	2013-06-19	08:29	23.9	179.9	0.5
2014	Worldview 3	2014-09-23	08:06	21.1	59.8	0.3
	UAV-based					
2014	camera	2014-10	Various	Various	Various	
	(orthomosaic)					0.1
2015	Pleiades-1A	2015-06-05	08:21	21.8	180.1	0.5
	UAV-based					
2015	camera	2015-10	Various	Various	Various	
	(orthomosaic)					0.1
2016	Pleiades-1A	2016-04-25	08:20	20.6	180.1	0.5
	UAV-based					
2016	camera	2016-11	Various	Various	Various	
	(orthomosaic)					0.1
2017	Pleiades-1A	2017-04-16	08:31	7.1	180.1	0.5
2018	Pleiades-1B	2018-04-23	08:23	19.6	180.1	0.5
2019	Pleiades-1B	2019-07-28	08:25	14.3	180.1	0.5
2020	Pleiades-1A	2020-04-12	08:33	27.1	180.1	0.5
2021	Pleiades-Neo	2021-08-18	08:14	25.7	97.9	0.3
2021	Pleiades-1A	2021-10-23	08:33	22.7	180.1	0.5
2022	Pleiades-1A	2022-01-29	08:28	7.2	180.1	0.5
2022	Pleiades-1B	2022-04-25	08:17	27.7	180.1	0.5
2022	Pleiades-Neo	2022-08-02	08:29	19.6	97.9	0.3
2023	Pleiades-1B	2023-11-08	08:29		128.9	0.5
2024	Pleiades-Neo	2024-01-22	12:18			0.3

Table S2: Pre-processing of the satellite images, including information regarding software utilisation for orthorectification and pansharpening, the Digital Elevation Model (DEM) used for the orthorectification, and any additional operations made using GDAL/OGR.

Year	Orthorectification and Pansharpening Software	DEM used in Orthorectification	Additional Georeferencing using GDAL/OGR?
1992	Aerial photography	n/a	n/a
2000	Aerial photography	n/a	n/a
2002	PCI	SRTM	Yes
2002	PCI	SRTM	Yes
2004	PCI	SRTM	Yes
2005	PCI	SRTM	Yes
2006	PCI	SRTM	Yes
2007	ERDAS	n/a	No
2008	ERDAS	n/a	No
2009	ERDAS	n/a	No
2010	ERDAS	n/a	No
2011	ERDAS	n/a	No
2012	PCI	ASTER	Yes
2012	ERDAS	n/a	No
2013	ERDAS	n/a	Yes
2014	PCI	JAXA	Yes
2015	ERDAS	n/a	Yes
2016	PCI	Elevation 30 (Airbus)	No
2017	PCI	Elevation 30 (Airbus)	No
2018	PCI	Elevation 30 (Airbus)	No
2019	ArcGIS pro	Elevation 30 (Airbus)	No
2020	ArcGIS pro	Elevation 30 (Airbus)	No
2021	ArcGIS pro	Elevation 30 (Airbus)	No
2021	ArcGIS pro	Elevation 30 (Airbus)	No
2022	ArcGIS pro	Elevation 30 (Airbus)	No
2022	ArcGIS pro	Elevation 30 (Airbus)	No
2022	ArcGIS pro	Elevation 30 (Airbus)	No
2023	n/a	n/a	No
2024	n/a	n/a	No

Supplementary Figures

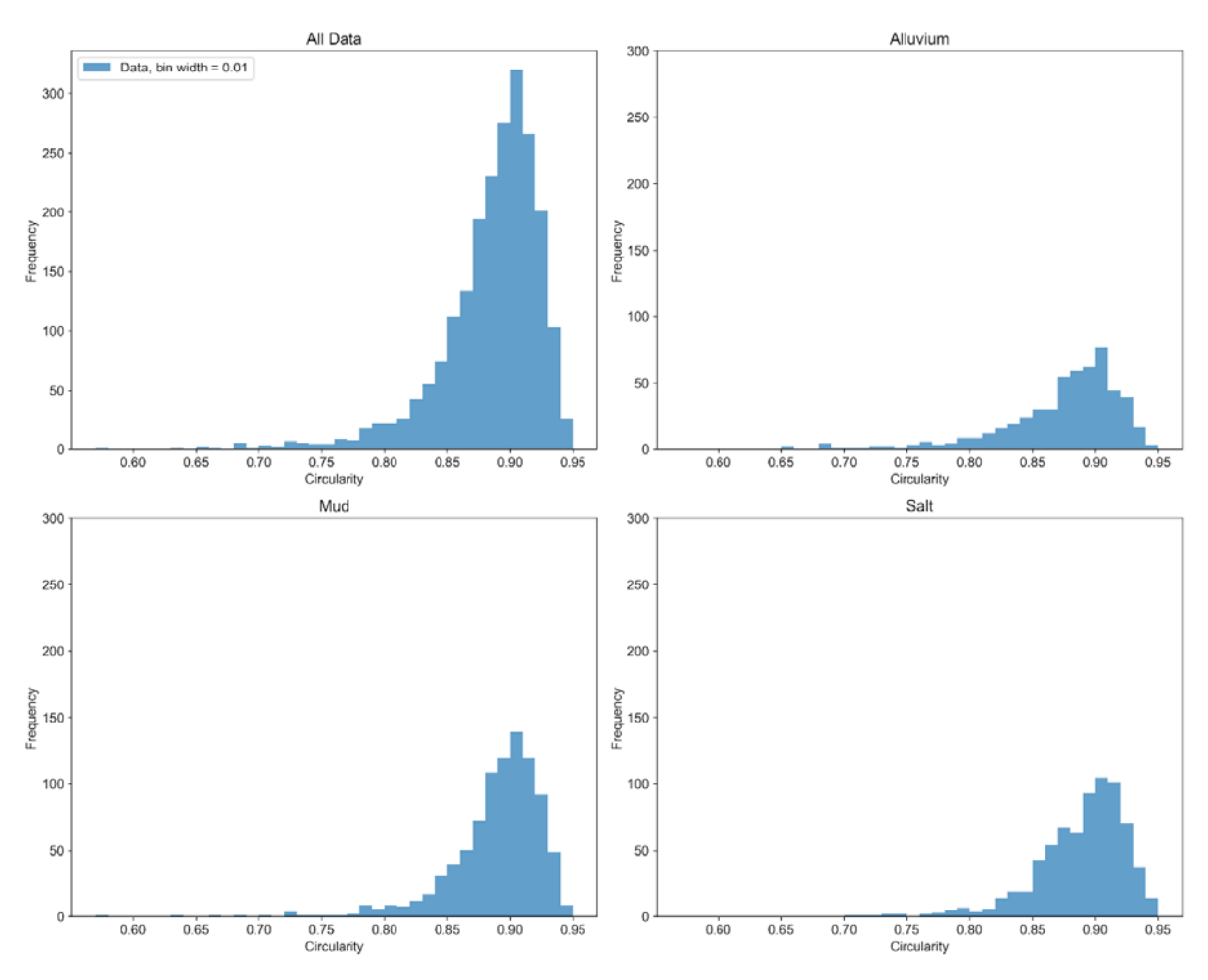


Figure S1: Circularity ratios for the sinkhole population. The ratio represents the relation between the area of the sinkhole and the area of a circle having a circumference equal to the perimeter of the sinkhole (equivalent area). A perfectly circular sinkhole has a circularity ratio of 1; as the irregularity of the sinkhole perimeter increases, the circularity ratio decreases.

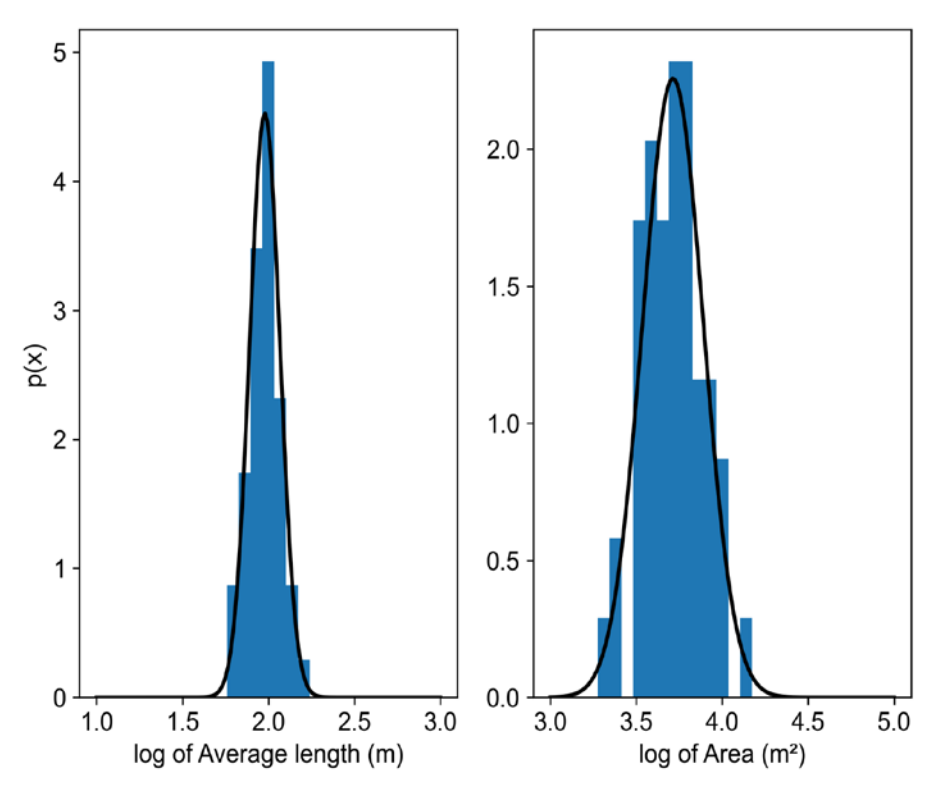


Figure S2: A first example of the distribution of the mean value of the log of 50 random subsets of sinkhole average length and area; n = 50 in both cases. For both length and area, the means of the log values are normally distributed, demonstrating that the data conform to the central limit theorem, though the visual fit for the area is not as good as for the average length.

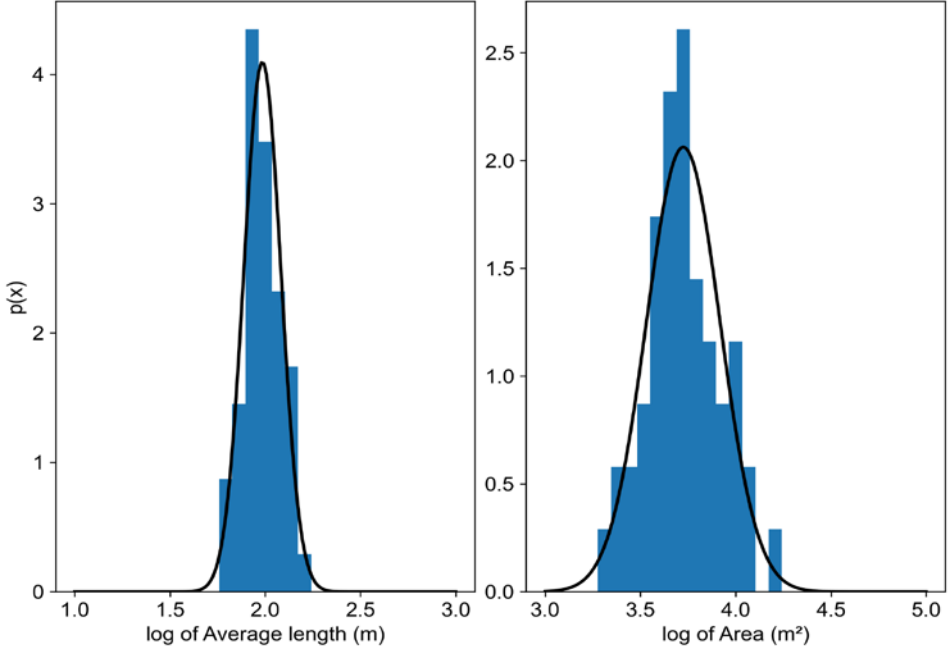


Figure S3: A second example of the distribution of the mean value of the log of 50 random subsets of sinkhole average length and area; n = 50 in both cases. For both length and area, the means of the log values are normally distributed, demonstrating that the data conform to the central limit theorem, though the visual fit for the area is not as good as for the average length.

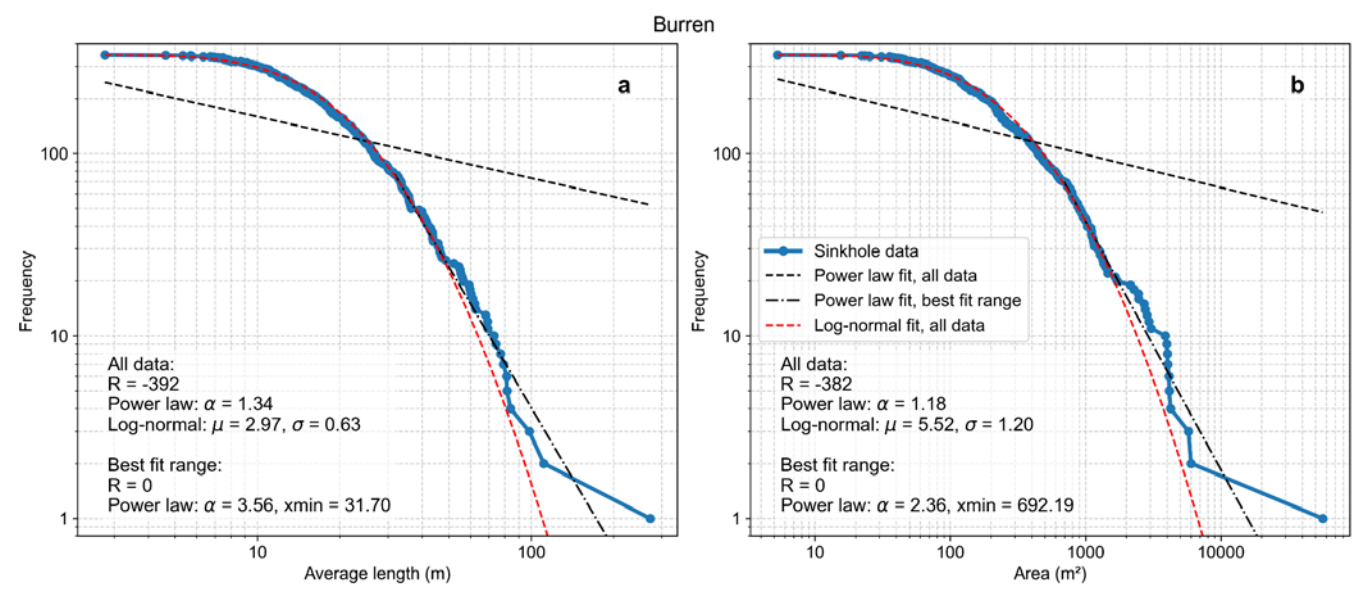


Figure S4: Cumulative frequency curves for (a) sinkhole average length and (b) sinkhole area for the Burren limestone karst in Ireland. In both cases, a power law fit can only be reasonably applied to the tail of the dataset (the larger sinkholes), whilst a lognormal fit reasonably approximates the entire distribution of sinkhole lengths and areas. The single largest sinkhole is a huge bedrock collapse sinkhole, Poll Berrin, which is something of an anomaly within the study area (cf. Watson et al., 2024).

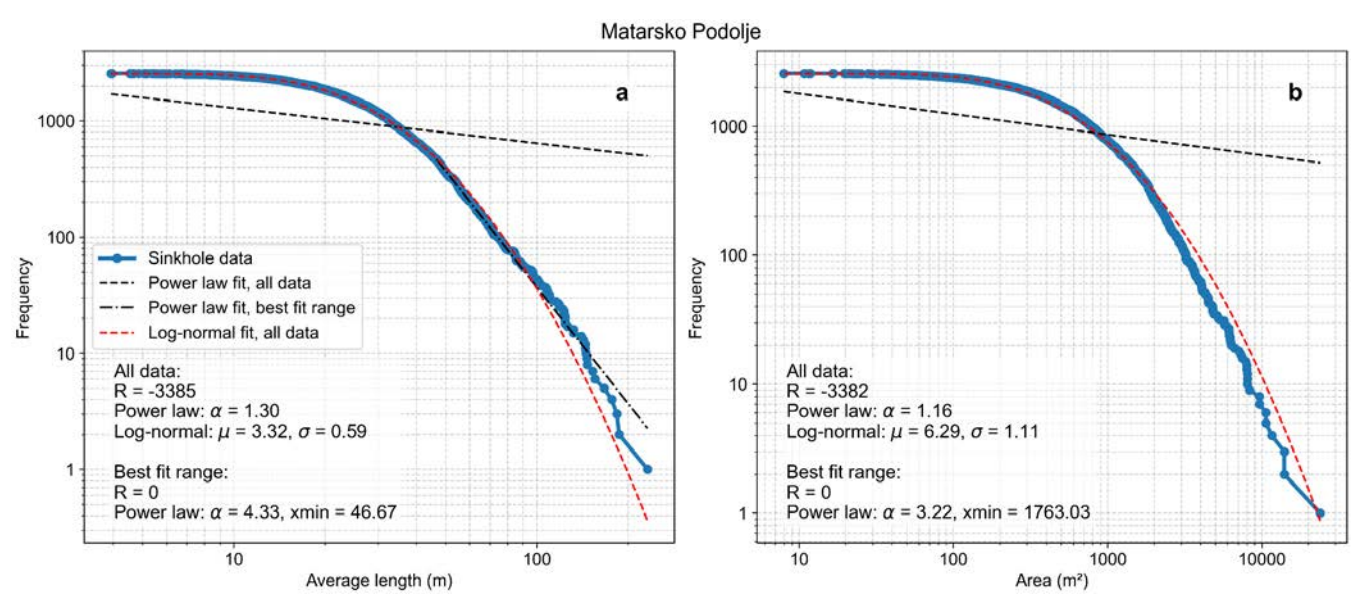


Figure S5: Cumulative frequency curves for (a) sinkhole average length and (b) sinkhole area for solution sinkholes from the Matarsko Podolje limestone karst area in Slovenia. In both cases, a power law fit can only be reasonably applied to the tail of the dataset (the larger sinkholes), whilst a lognormal fit reasonably approximates the entire distribution of sinkhole lengths and areas.

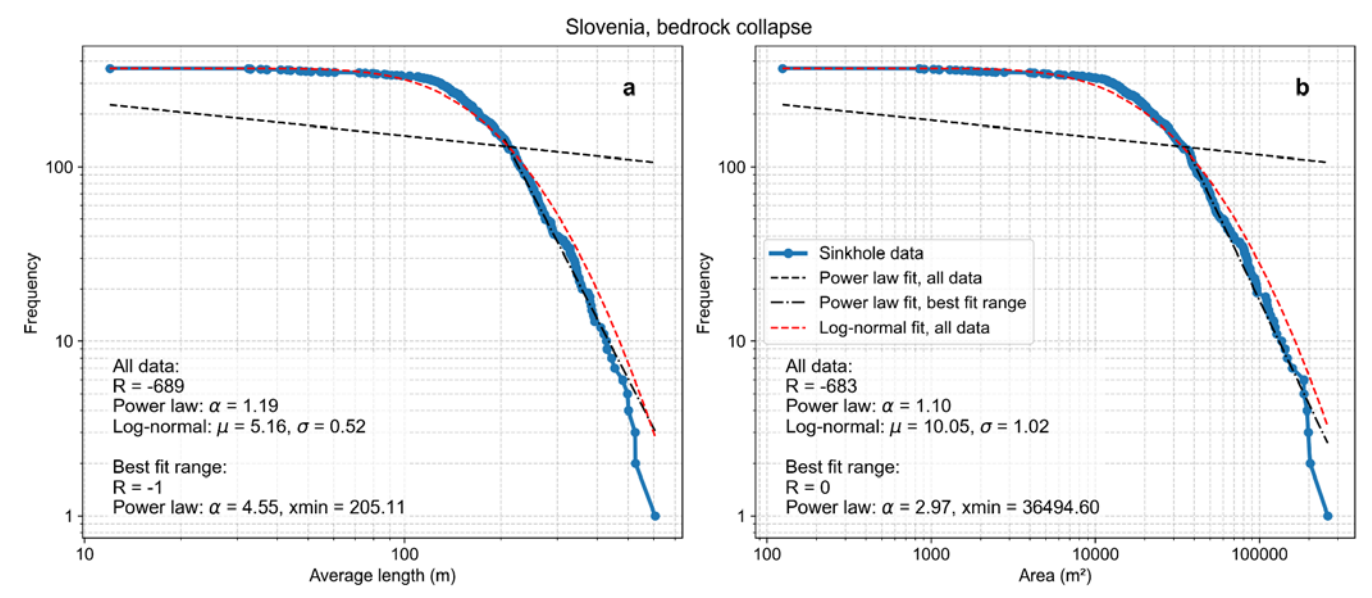


Figure S6: Cumulative frequency curves for (a) sinkhole average length and (b) sinkhole area for bedrock collapse sinkholes from karst areas across Slovenia. In both cases, a power law fit can only be reasonably applied to the tail of the dataset (the larger sinkholes), whilst a lognormal fit reasonably approximates the entire distribution of sinkhole lengths and areas.

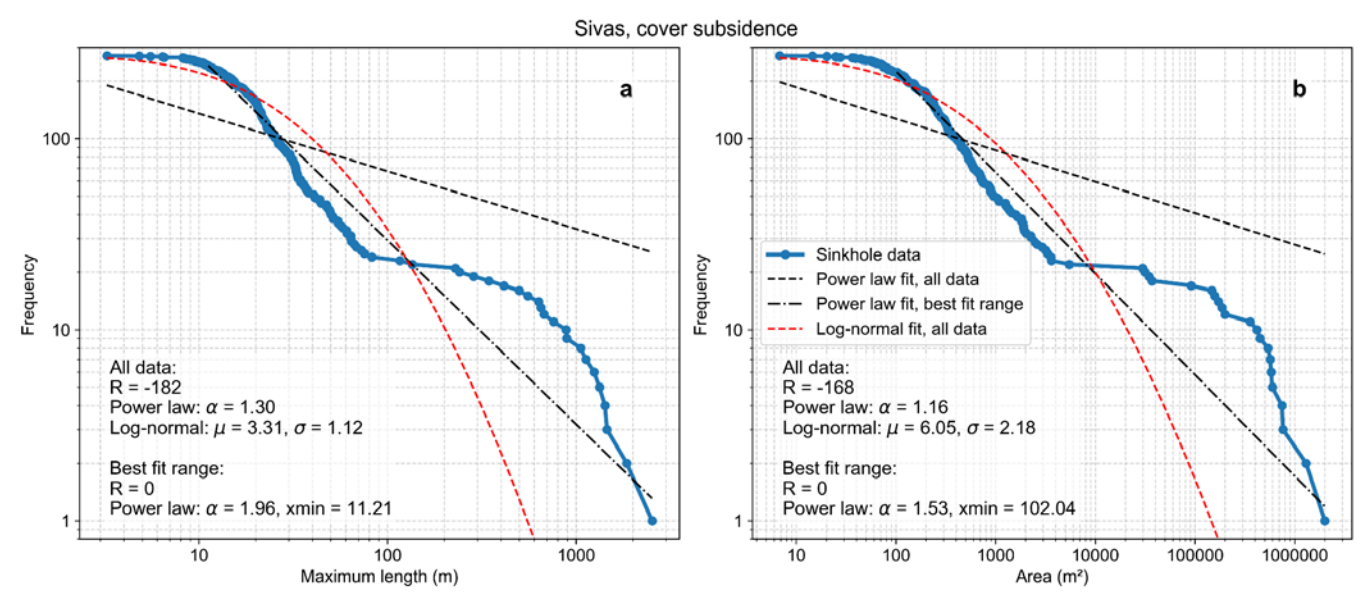


Figure S7: Cumulative frequency curves for (a) sinkhole average length and (b) sinkhole area for cover subsidence sinkholes from the Sivas gypsum karst in Turkiye.

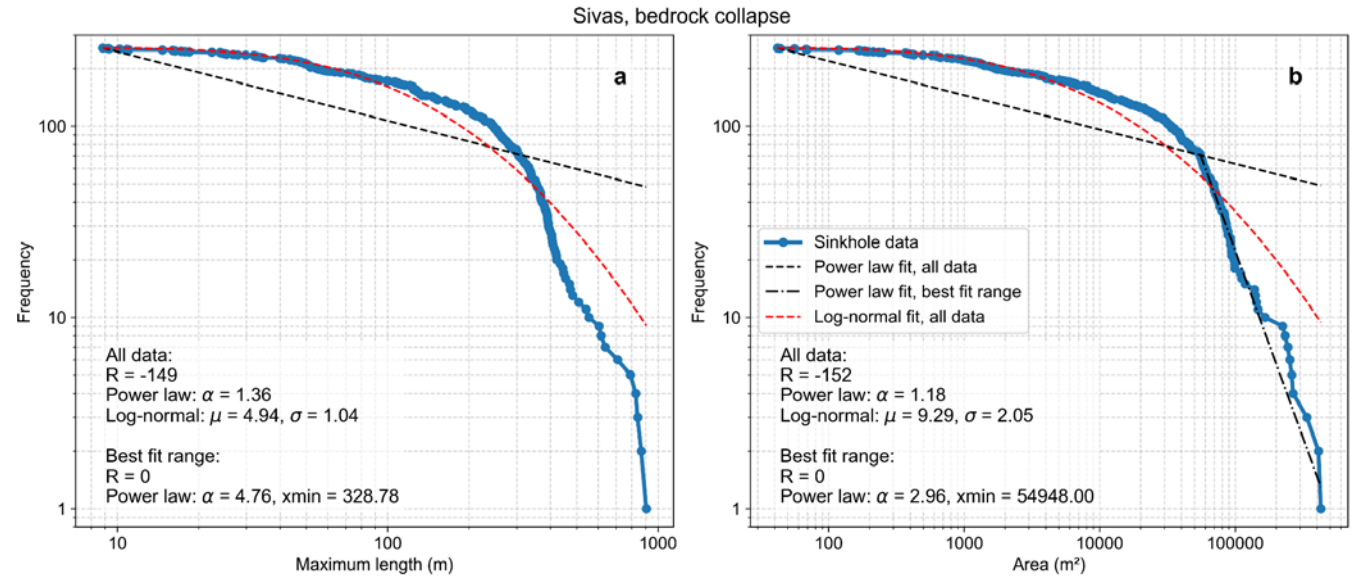


Figure S8: Cumulative frequency curves for (a) sinkhole average length and (b) sinkhole area for bedrock collapse sinkholes from the Sivas gypsum karst in Turkiye.